Supporting Information

1D Pb Halide Perovskite-like Materials for High Performance X-ray Detection

Jing Wang,[a,b] Jin-Hai Yang,[a] Jie Chen,[a,d] Shuai-Hua Wang,*[a,d] Yong-Jun Chen,*[a] and Gang Xu[acd]

[a]*State Key Laboratory of Structural Chemistry, and Fujian Provincial Key Laboratory of Materials and Techniques toward Hydrogen Energy, Fujian Institute of Research on the Structure of Matter, Chinese Academy of Sciences, Fuzhou 350002, China.*
[b]*College of Chemistry and Materials Science, Fujian Normal University, Fuzhou, Fujian 350007, China.*
[c]*Science & Technology Innovation Laboratory for Optoelectronic Information of China, Fuzhou 350108, China.*
[d]*University of Chinese Academy of Science (UCAS), Beijing 100049, China.*

Corresponding author: *S-H. Wang (E-mail: shwang@fjirsm.ac.cn) and Y-J. Chen (E-mail: chenyongjun@fjirsm.ac.cn).*

Methods

Raw materials

All solvents and reagents obtained from commercial sources were used without further purification. Lead dichloride ($PbCl_2$, 99.5%), lead bromide ($PbBr_2$, 99.5%) and lead iodide (PbI_2, 99.5%) were purchased from Aladdin (Shanghai). 6,6'-dithiodinicotinic acid (DTDA, 99%) was purchased from TCI (Shanghai). Hydrochloric acid (HCl, 36% in water) was purchased from Sinopharm Chemical Reagent Co., Ltd. Hydrobromic acid (HBr, 48% in water) was obtained from General-reagent. Hydroiodic acid solution (HI, 56% in water) was purchased from Damas-beta. Hypophosphorous acid (H_3PO_2, 50% in water) were purchased from Macklin.

Synthesis of single crystals 1, 2, and 3

$PbCl_2$ (0.08 g, 0.3 mmol), DTDA (0.06 g, 0.2 mmol), HCl (6 mL) and H_3PO_2 (1 mL) were mixed in a round-bottom flask. After appropriate stirring and heating, the mixture became clear solution. Then, the light rod single crystal of **1** was obtained by slowly cooling the solution in a blast oven for 1 h. The synthesis process of single crystals of **2** and **3** was similar to that of **1**, except that $PbCl_2$ (0.08 g, 0.3 mmol) was replaced by $PbBr_2$ (0.3 g, 0.82 mmol) and PbI_2 (0.3 g, 0.65 mmol) respectively, and HCl (6 mL) was replaced by HBr (8 mL) and HI (8 mL) respectively. Finally, the single crystals of **2** and **3** were obtained.

Single-crystal X-ray diffraction structure determination

The single crystal diffraction date was collected by using a Bruker D8 Quesr/Venture diffractometer with the Mo Kα radiation (λ = 0.77 Å). The structure was solved by direct methods and confirmed by the full-matrix least-squares refinements on F2 using the SHELXTL software packing. All non-H atoms were refined anisotropically and all H atoms were generated by geometrical method. Then all atoms were refined by using a "riding" model with Uiso = 1.2 Ueq (C). The above-mentioned structure solution and refinement were conducted in the Olex2 software. Crystallographic data for single crystals **1**, **2**, and **3** reported in this paper have been deposited in the Cambridge Crystallographic data Centre with CCDC 2314917-2314919.

Characterization

Powder X-ray diffraction (PXRD) patterns of samples were obtained using a D/max 2500 VL/PC diffractometer (Japan) equipped with Cu Kα radiation (λ = 1.54060 Å). The thermo-gravimetric analysis for samples were conducted on a STA449F3 Jupiter simultaneous thermal analyzer (NETZSCH STA449C) under a nitrogen atmosphere from room temperature to 1000 °C with a rate of 10 °C min^{-1}. The UV-Visible absorption spectrum in the solid state was measured at room temperature on a PE Lambda 950 UV-visible-NIR spectrophotometer.

DFT calculations

First-principles density function theory (DFT) calculations were performed using the plane-wave pseudopotential method implemented in the Cambridge Sequential Total Energy Package (CASTEP). The exchange-correlation potential was calculated using the Perdew-Burke-Ernzerhof for solids (PBEsol) functional within the generalized gradient approximation (GGA). The interactions between the ionic cores and the electrons were described by the norm-conserving pseudopotential. Photoelectric measurements were performed with a crystalline electrode configuration.

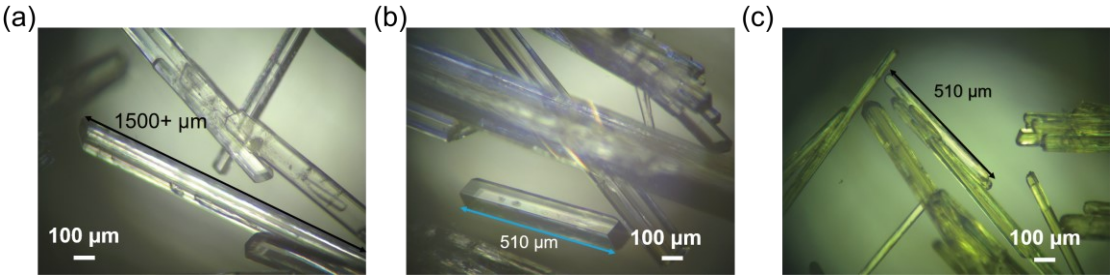

Fig. S1 Microscopic optical photographs of **1** (a), **2** (b) and **3** (c).

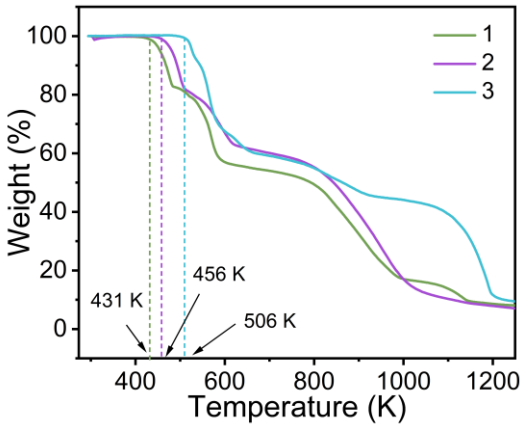

Fig. S2 Thermal stability of single crystals. These crystals of **1**, **2** and **3** can be stable at temperatures as high as 431 K, 456 K and 506 K, respectively.

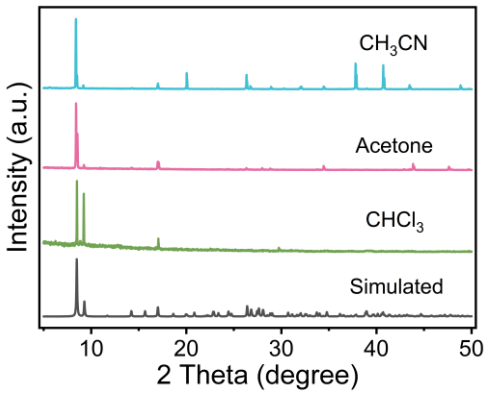

Fig. S3 Chemical stability of **3**. We studied the chemical stability of the samples taking **3** for an example. The structural integrity of **3** remained unchanged in common organic solvents, including CH_3CN, acetone, and $CHCl_3$ for more than 12 has revealed by PXRD tests.

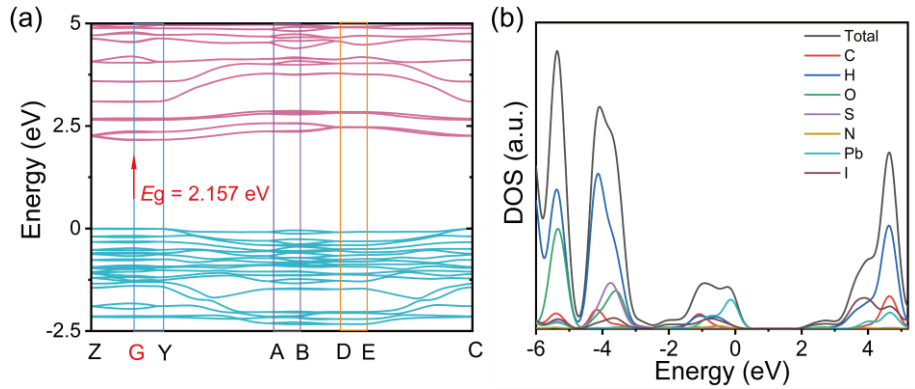

Fig. S4 (a) Calculated band gap of **3**; (b) Band structure and density of states. For semiconductor materials, the reduced bandgap results in a smaller range of electron motion in the energy band, enhancing the interaction between electrons, which brings higher electron mobility. In addition, the semiconductors with smaller bandgap have narrower range of energy absorption for light, resulting in higher absorption for specific wavelengths of light to bring stronger light absorption.

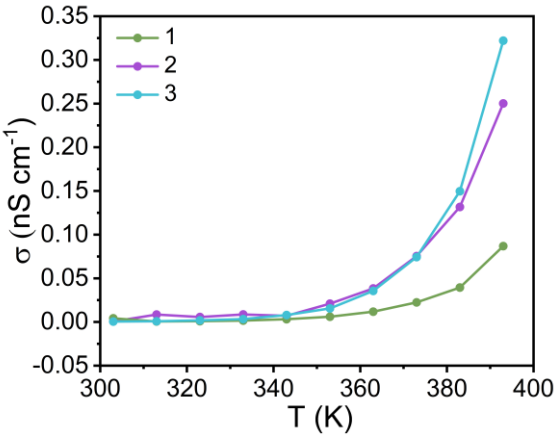

Fig. S5 Variable temperature conductivity of **1**, **2** and **3**.

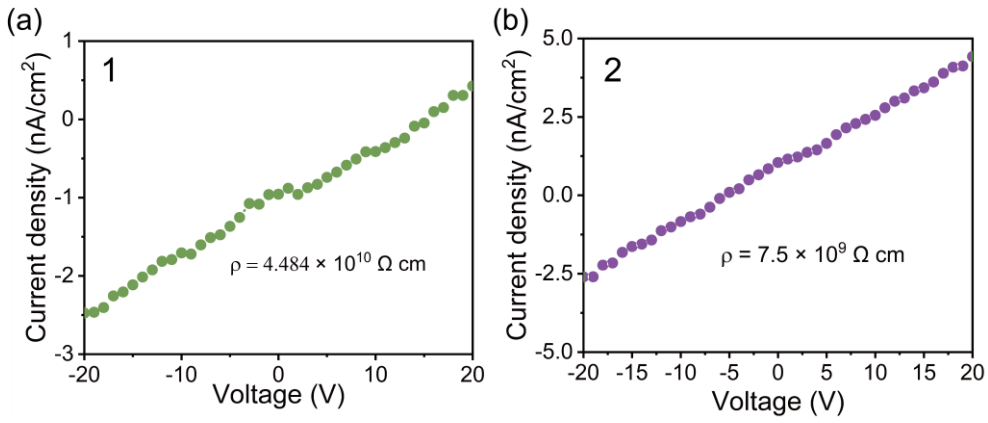

Fig. S6 Bulk resistivity of **1** (a) and **2** (b).

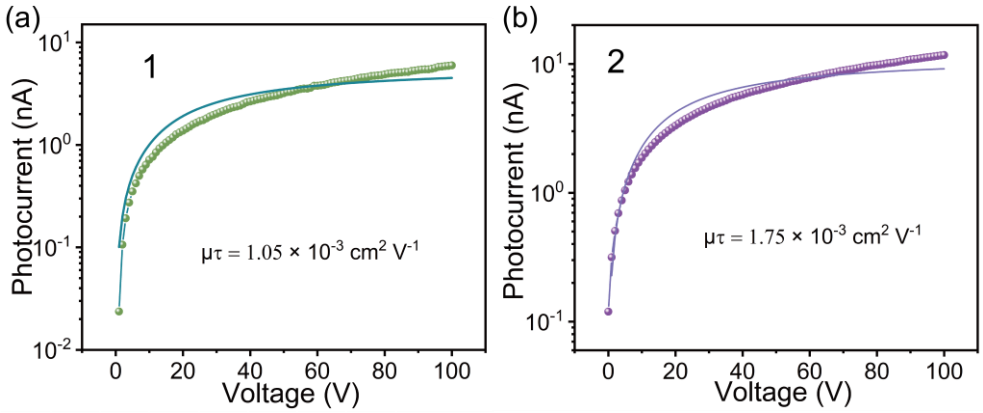

Fig. S7 The voltage-dependent photocurrent of **1** (a) and **2** (b) under X-ray irradiation. The $\mu\tau$ product was derived by fitting the photoconductivity based on the simplified Hecht equation.[1]

$$I = \frac{I_0 \mu\tau V}{L^2}[1 - \exp(\frac{-L^2}{\mu\tau V})] \quad (1)$$

where I_0 is the saturated photocurrent, I is the photocurrent, L is the thickness, V is the applied bias, μ is carrier mobility, and τ is carrier lifetime.

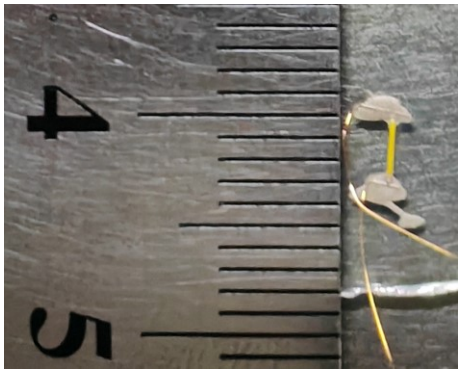

Fig. S8 X-ray detection device of **3**.

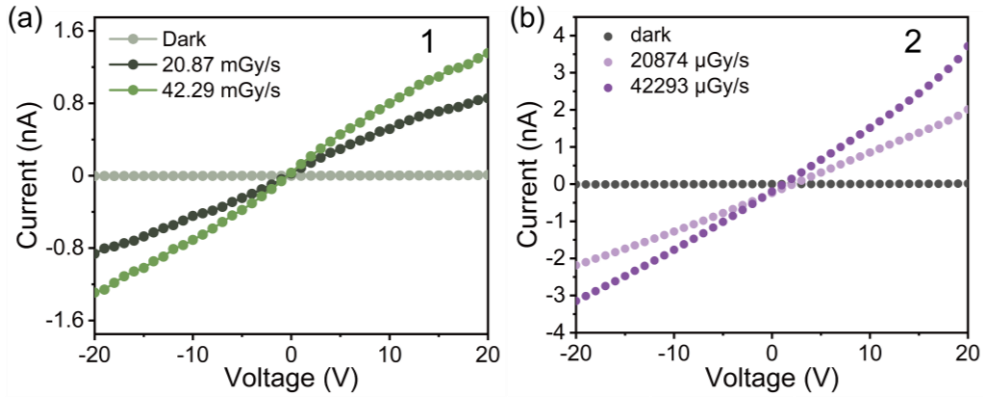

Fig. S9 *I-V* traces of **1** (a) and **2** (b) detector in dark and under X-ray irradiation.

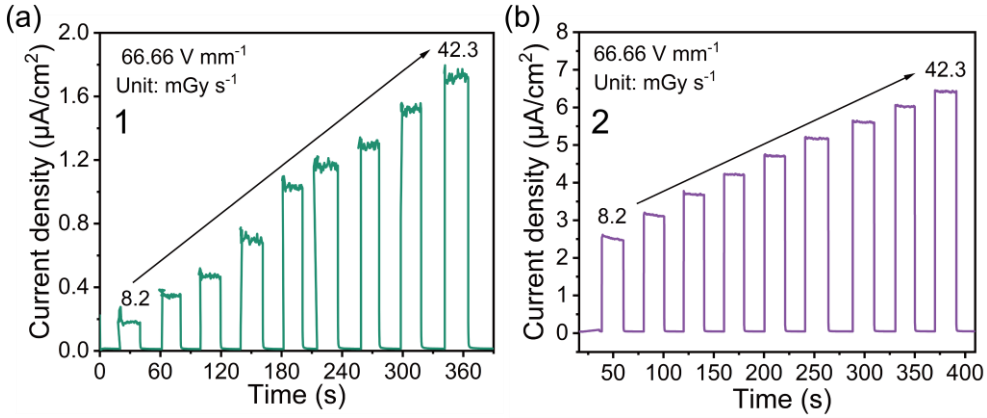

Fig. S10 Current density of **1** (a) and **2** (b) detector to X-ray with increased dose rates.

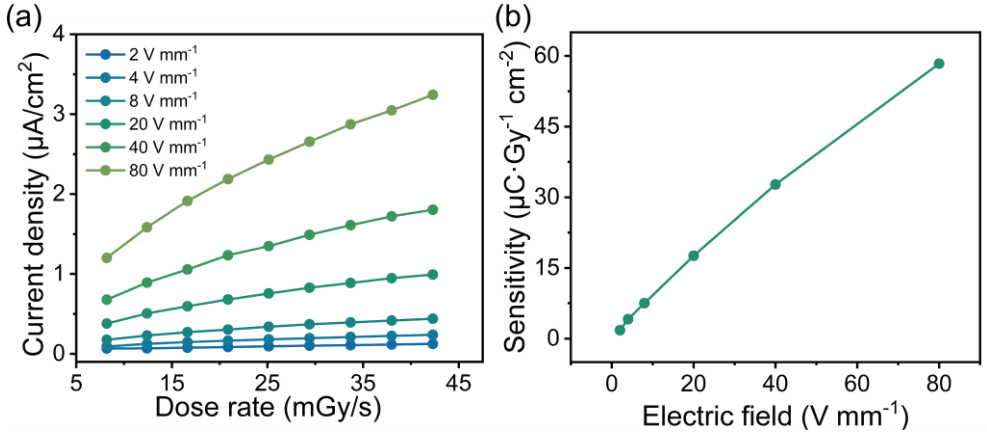

Fig. S11 (a) Linearly fitted current density and X-ray dose rate to obtain sensitivity at different biases; (b) Sensitivity of **1** detector under different electric fields.

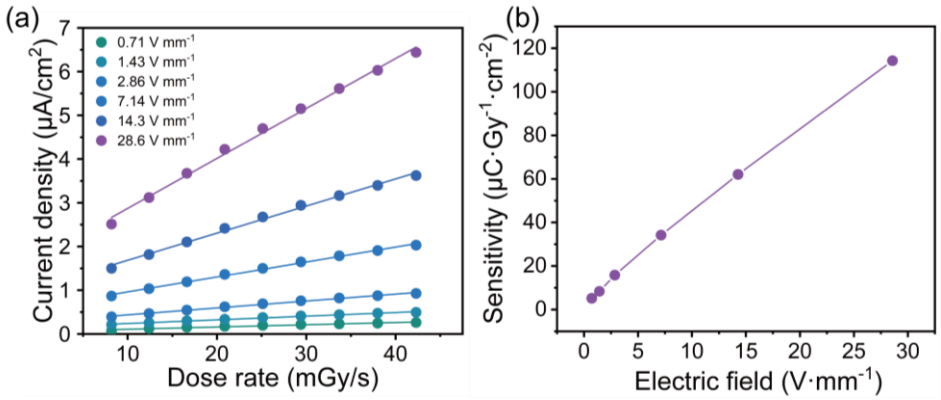

Fig**.** S12 (a) Linearly fitted current density and X-ray dose rate to obtain sensitivity at different biases; (b) Sensitivity of **2** detector different electric fields.

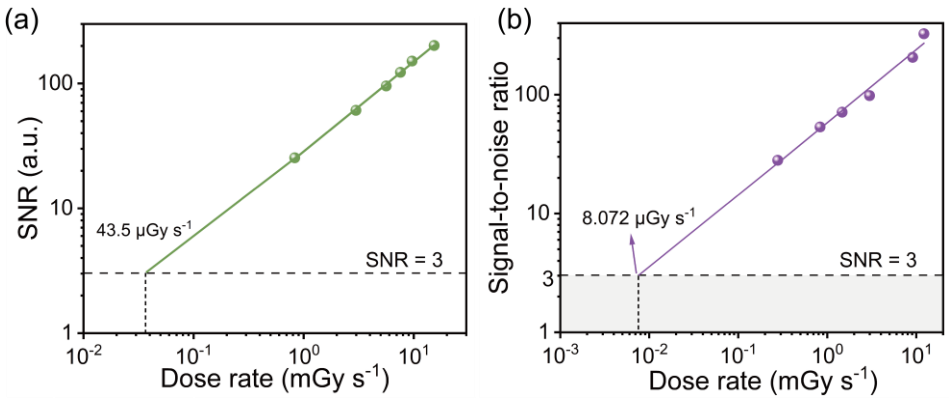

Fig. S13 Signal-to-noise ratio (SNR) of **1** (a) and **2** (b) at 50 V.

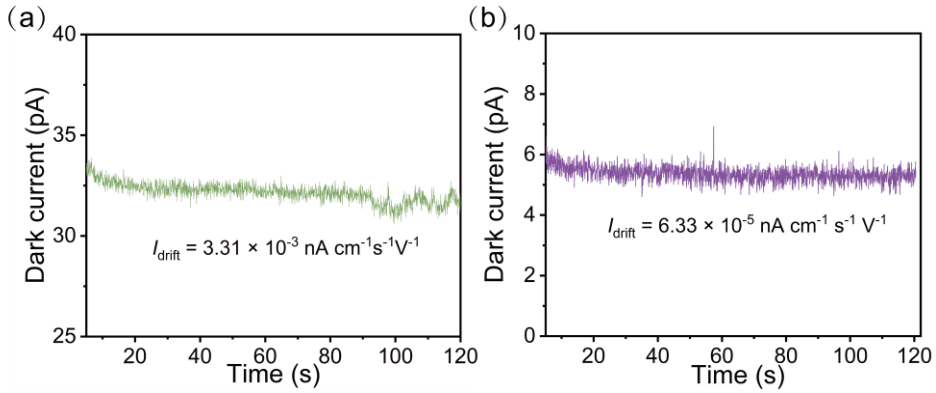

Fig. S14 Bulk resistivity of **1** (a), **2** (b). The I_{drift} is determined through the following equation[2]

$$I_{drift} = (I_t - I_0) / (E \times S \times t) \quad (2)$$

where E is electric field, S is the device area, the I_t and I_0 are dark current at time t and 0, respectively.

Table S1. Crystal data of three crystals received near room temperature.

Empirical formula	$C_{12}H_{12}Cl_4N_2O_4PbS_2$	$C_{12}H_{12}Br_4N_2O_4PbS_2$	$C_{12}H_{12}I_4N_2O_4PbS_2$
Formula weight	663.36	839.19	1027.15
Temperature/K	265.61	299.97	299.9
Crystal system	monoclinic	monoclinic	monoclinic
Space group	$P2_1/c$	$P2_1/c$	$P2_1/c$
a/Å	4.3263(3)	4.4621(4)	4.6903(3)
b/Å	18.5138(16)	19.0334(17)	19.9065(16)
c/Å	12.3948(13)	12.5804(13)	12.8200(11)
α/°	90	90	90
β/°	97.504(3)	98.489(4)	99.393(3)
γ/°	90	90	90
Volume/Å^3	984.27(15)	1056.73(17)	1180.92(16)
Z	2	2	2
ρ_{calc}g/cm^3	2.238	2.637	2.889
μ/mm^{-1}	9.345	15.762	12.566
F(000)	628.0	768.0	912.0
Radiation	MoKα (λ = 0.77)	MoKα (λ = 0.77)	MoKα (λ = 0.77)
2Θ range for data collection/°	6.988 to 55.442	6.55 to 55.056	6.76 to 55.014
Reflections collected	16673	15564	21338
Independent reflections	2294 [R_{int} = 0.0626, R_{sigma} = 0.0336]	2435 [R_{int} = 0.0800, R_{sigma} = 0.0497]	2705 [R_{int} = 0.0562, R_{sigma} = 0.0300]
Data/restraints/parameters	2294/0/117	2435/1/120	2705/0/117
Goodness-of-fit on F^2	1.051	1.027	1.082
Final R indexes [I>=2σ (I)]	R_1 = 0.0234, wR_2 = 0.0472	R_1 = 0.0318, wR_2 = 0.0565	R_1 = 0.0247, wR_2 =0.0469
Final R indexes [all data]	R_1 = 0.0385, wR_2 = 0.0540	R_1 = 0.0610, wR_2 = 0.0673	R_1 = 0.0369, wR_2 =0.0522
Largest diff. peak/hole / e Å^{-3}	0.53/-0.70	0.69/-0.83	0.66/-0.55

Table S2. The D-H···A Hydrogen bond of **1**

D-H	d(D-H)	d(H···A)	<DHA	d(D···A)	A
S04-H04	1.200	2.916	129.89	3.799	Cl02
O006-H006	0.820	1.808	173.14	2.624	O005[-x, -y+1, -z+2]
N007-H007	0.860	2.199	173.32	3.055	Cl02
C008-H008	0.930	2.892	146.64	3.704	Cl03[x-1, -y+3/2, z+1/2]
C00D-H00D	0.930	2.629	166.11	3.539	Cl03[-x+2, -y+1, -z+1]

Table S3. The D-H···A Hydrogen bond of **2**

D-H	d(D-H)	d(H···A)	<DHA	d(D···A)	A
S004-H004	1.200	2.905	130.35	3.794	Br02
N005-H005	0.860	2.372	174.01	3.228	Br02
C008-H008	0.930	2.765	164.00	3.668	Br03
C00B-H00B	0.930	3.123	145.15	3.922	Br03[-x+1, y+1/2, -z+1/2]
O006-H006	1.001	1.642	175.16	2.640	O007[-x, -y+1, -z+1]

Table S4. The D-H···A Hydrogen bond of **3**

D-H	d(D-H)	d(H···A)	<DHA	d(D···A)	A
S004-H004	1.200	2.890	145.20	3.936	I003[-x-1, y+1/2, -z+3/2]
O005-H005	0.820	1.893	153.77	2.654	O007[-x+2, -y+1, -z+1]
N006-H006	0.860	2.607	172.91	3.462	I002
C009-H009	0.930	3.280	127.34	3.915	I002[x+1, -y+3/2, z-1/2]
C00B-H00B	0.930	2.983	164.69	3.888	I003

Reference

1 W. Pan, B. Yang, G. Niu, K.-H. Xue, X. Du, L. Yin, M. Zhang, H. Wu, X.-S. Miao and J. Tang, *Adv. Mater.*, 2019, **31,** 1904405.

2 X. Guo, Z. Gao, C. Li, J. Zhang and X. Tao, *Adv. Funct. Mater.*, 2023, **33**, 2301002.